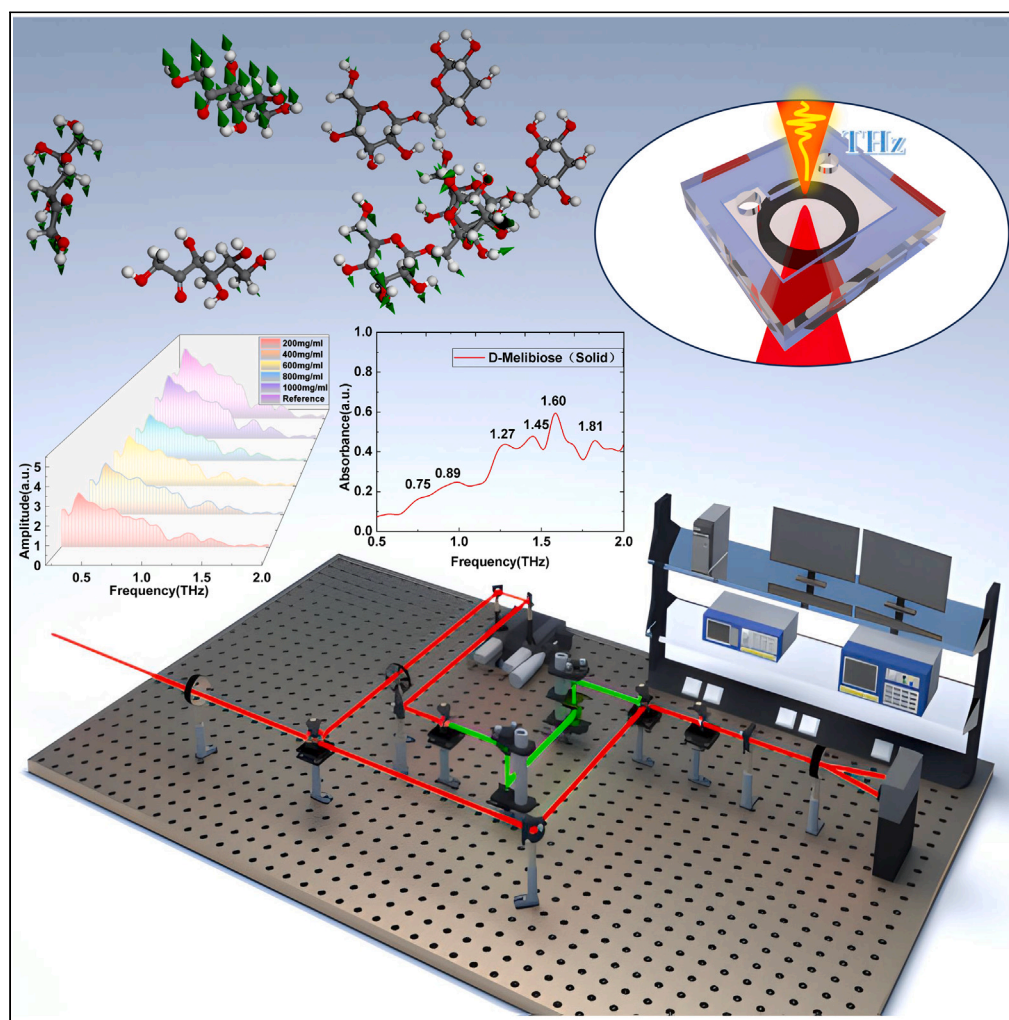**Article**

Exploring terahertz spectral characteristics of L-sorbose and D-melibiose in solid and liquid states

Boyan Zhang, Yuhan Zhao, Jingyi Shu, ..., Siyu Qian, Bo Su, Cunlin Zhang

subo75@cnu.edu.cn

Highlights

Solid L-sorbose and D-melibiose have unique absorption peaks

The simulation and experimental results of the two saccharides are consistent

The THz spectra of the two saccharides in solid and aqueous solutions are correlated

The absorption spectra of the two saccharides are temperature dependent

Article

Exploring terahertz spectral characteristics of L-sorbose and D-melibiose in solid and liquid states

Boyan Zhang,[1,2,3,4] Yuhan Zhao,[1,2,3,4] Jingyi Shu,[1,2,3,4] Bingxin Yan,[1,2,3,4] Bo Peng,[1,2,3,4] Siyu Qian,[1,2,3,4] Bo Su,[1,2,3,4,5,*] and Cunlin Zhang[1,2,3,4]

SUMMARY

Saccharides are essential organic compounds that perform critical functions in sustaining life processes. As biomolecules, their vibrational frequencies predominantly fall in the terahertz (THz) range, making them amenable to analysis using THz techniques. In this study, L-sorbose and D-melibiose were measured using a THz time-domain spectroscopy system covering a frequency range of 0.1–2.0 THz, and their crystal structures were simulated using density functional theory. The experimental results demonstrated significant agreement with the simulation findings. In addition, the spectral properties of the two saccharides in solution were determined using microfluidic chip technology, thereby facilitating a comparison between the solid and aqueous states. The results demonstrate that the intramolecular and intermolecular interactions of the saccharides were weakened by the presence of water molecules, and the THz absorption spectrum of the same substance solution was found to be correlated with its concentration and temperature.

INTRODUCTION

Terahertz (THz), also referred to as far-infrared radiation, is an electromagnetic wave with a high frequency typically ranging from 0.1 to 10 THz and a wavelength ranging from 3,000 to 30 μm.[1–3] The development of ultrafast laser and semiconductor technologies has led to a reliable and stable excitation source for the generation of THz waves, enabling a wide range of safety detection, biomedicine, and spectroscopy applications. The low energy of THz photons makes them suitable for nondestructive material testing as they cannot ionize the sample.[4,5] THz spectroscopy has been used extensively to identify molecular structures due to its high sensitivity to both the molecule itself and any changes in its structure. Many organic molecules, including saccharides, exhibit rich and unique spectra in the frequency range below 4 THz.

The study of saccharides has gained increasing attention since the concept of glycobiology was introduced,[6] and glycan chemistry has shifted from organic chemistry to a combination of organic chemistry and biology. Saccharides have penetrated biochemical reaction processes, e.g., the recognition of growth and development genetics by immune molecules. Saccharide molecules undergo vibration through bond stretching, bending, and relative motion between molecules, enabling their detection and identification using THz technology.[7,8] For example, L-sorbose is a readily available natural saccharide widely found in fruits that is used in food additives to improve the moisturizing properties of foods.[9,10] It has also been widely used in vitamin C synthesis and metabolic studies in animals and microorganisms.[11,12] D-melibiose is a natural oligosaccharide contained in many plants that can reduce the symptoms of allergic dermatitis while improving the body's immunity to fight inflammation.[13] The different chiral spectral characteristics of the same saccharide are generally similar, but different saccharides have different spectral absorption in THz band.[14] Thus, THz spectroscopy is a feasible approach for understanding the fundamental properties of different saccharides, including their spectral characteristics in different frequency ranges.[15] Upadhya et al. utilized THz time-domain spectroscopy (THz-TDS) to investigate two therapeutic biomolecules,[16] i.e., glucose and uric acid, and they proposed stereoisomers of both based on the intermolecular vibrational modes exhibited in their spectral features. In addition, Zhang et al. conducted a high-resolution THz spectroscopic study on two structural isomers, mannose and galactose, and they found significant differences between these closely related molecules at room temperature within 0.5–4.0 THz frequencies.[17] While previous studies have explored the THz or infrared absorption spectra of various saccharides, most of these investigations focused on the measurement of solid substances or making theoretical calculations on isolated molecules and analyzing the origin of the absorption features. However, the main functions of biomolecules in glycobiology are realized in aqueous solutions, and direct identification of aqueous solutions of saccharides
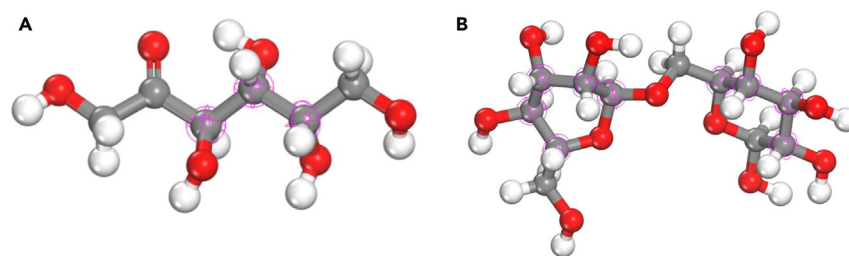
Figure 1. Structural formulas of L-sorbose and D-melibiose (Purple rings are chiral carbon atoms)
(A) L-sorbose.
(B) D-melibiose.

with THz-TDS has not been investigated extensively, primarily due to the strong absorption of THz via hydrogen bonding in water.[18] Thus, studying the THz absorption spectra of saccharides in both solid and liquid states, as well as their vibrational modes, is crucial in practical glycobiology.

Microfluidics technology can accurately manipulate microscale fluids and has been widely used in chemical, physical, and biological detection fields due to its various advantages such as low liquid sample consumption, fast detection speed, and easy operation.[19] Therefore, we used the Zeonor 1420R material with high transmittance to THz waves to fabricate a sandwich microfluidic chip and designed a temperature control device to independently regulate the temperature of the internal liquid.

In this paper, we selected L-sorbose and D-melibiose, which are extensively utilized in the fields of biology and pharmaceuticals, as our subjects of study. Firstly, we investigated their solid-state THz spectra and carried out molecular dynamics simulation, showing a strong agreement between theoretical simulation and experimental results. Subsequently, we employed our specifically designed microfluidic chip to detect these two saccharide solutions, effectively reducing the interaction distance between THz waves and the solutions. Lastly, we compared the changes in absorption spectra between the solid and solution states and examined the impact of varying temperatures and concentrations on the THz spectra of these saccharide solutions. Our study offers a detailed analysis of the THz spectral characteristics of L-sorbose and D-melibiose from multiple perspectives, unveiling the influence of the surrounding environment on molecular vibration modes.
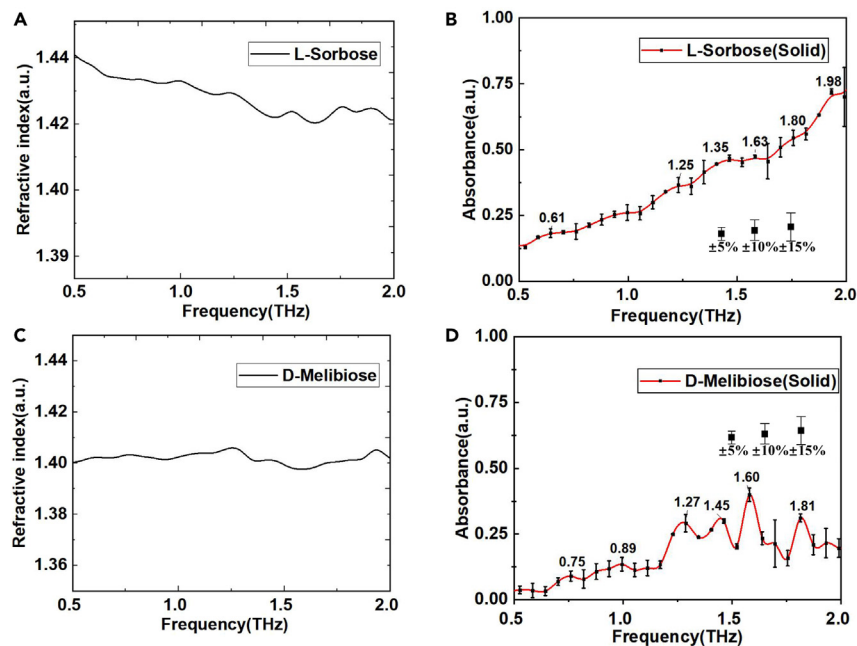

Figure 2. THz spectra of solid L-sorbose and D-melibiose
(A) L-sorbose refractive index spectrum.
(B) L-sorbose absorption coefficient spectrum.
(C) D-melibiose refractive index spectrum.
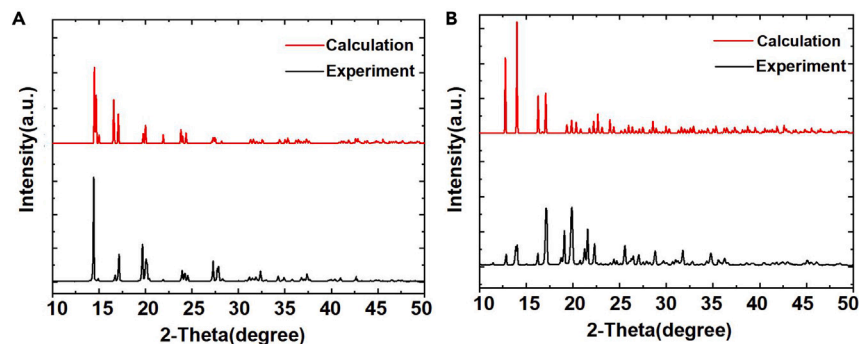(D) D-melibiose absorption coefficient spectrum.

Figure 3. Comparison between PXRD experiment and calculation pattern
(A) L-sorbose (B) D-melibiose.

RESULTS AND DISCUSSION

THz spectra of solid saccharides

The structures of the L-sorbose and D-melibiose are shown in Figure 1. A fast Fourier transform of the time-domain profiles of the sample and reference signals gives their refractive index and absorption coefficient profiles. Figure 2 shows the THz spectra of the L-sorbose and D-melibiose as solids at room temperature. As can be seen, the L-sorbose exhibits six distinctive absorption peaks in the 0.2–2.0 THz band at frequencies of 0.61, 1.25, 1.35, 1.63, 1.80, and 1.98 THz, with different peak intensities due to different peak generation mechanisms. The D-melibiose exhibits six absorption peaks at 0.75, 0.89, 1.27, 1.45, 1.60, and 1.81 THz. In order to ensure the authenticity of the experimental data, we repeated the experiment for more than three times in each group of the aforementioned experiments. At the same time, we have incorporated error bars into the THz spectra. These error bars show that our error is small, which further proves the robustness and high feasibility of our experimental method. The Fourier-transformed spectra of the sample and the reference group can be seen in Figure S1. The refractive indices of the L-sorbose were in the range of 1.40–1.45, and those of the D-melibiose were in the range of 1.39–1.41. The refractive
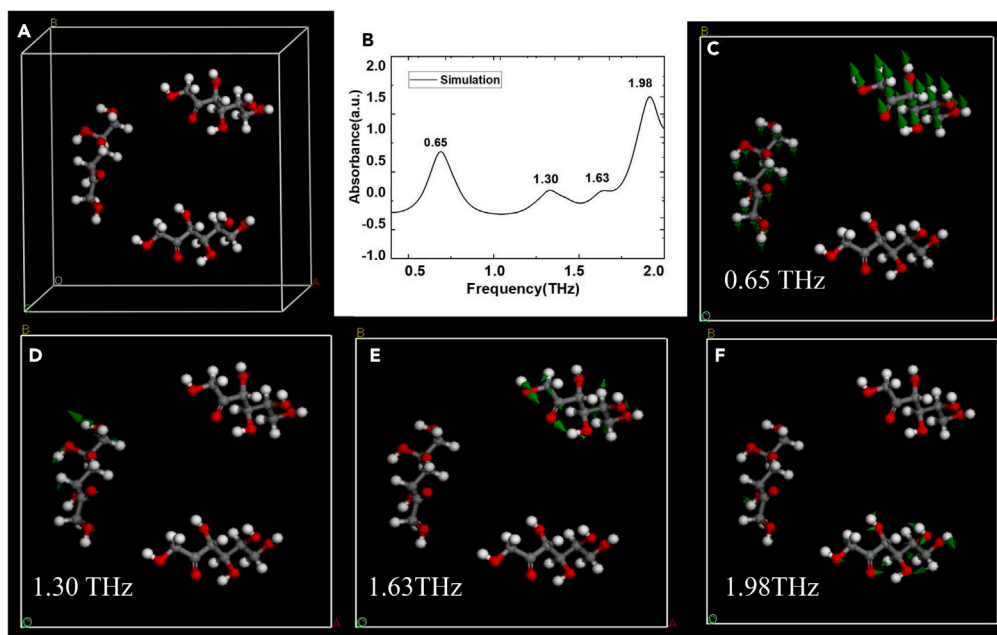

Figure 4. Simulated results of the THz spectrum and the corresponding vibrational modes of L-Sorbose
(A) Crystal structure of L-sorbose.
(B) Simulation spectrogram of L-sorbose.
(C) Vibration mode of L-sorbose at 0.65 THz.
(D) Vibration mode of L-sorbose at 1.30 THz.
(E) Vibration mode of L-sorbose at 1.63 THz.
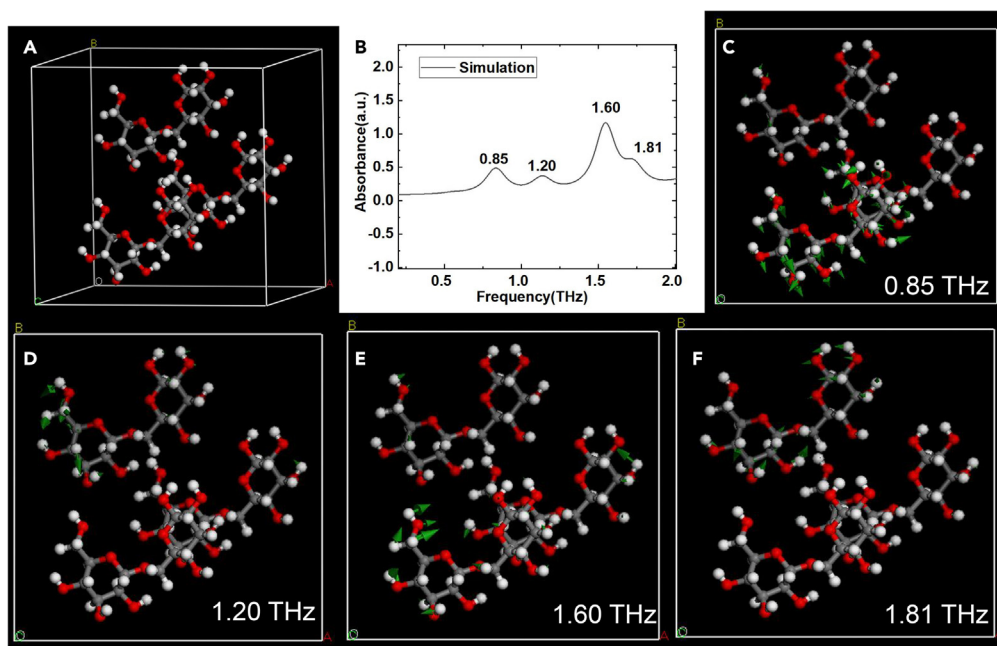(F) Vibration mode of L-sorbose at 1.98 THz.

Figure 5. Simulated results of the THz spectrum and corresponding vibrational modes of D-melibiose
(A) Crystal structure of D-melibiose.
(B) Simulation spectrogram of D-melibiose.
(C) Vibration modes at 0.85 THz of D-melibiose.
(D) Vibration modes at 1.20 THz of D-melibiose.
(E) Vibration modes at 1.60 THz of D-melibiose.
(F) Vibration modes at 1.81 THz of D-melibiose.

indices at the positions where the absorption peaks appeared decreased with increasing frequency, i.e., anomalous dispersion occurred, which is consistent with the Kramers-Kronig relationship.

Simulation of solid saccharides

To gain insights into the spectra mechanism of the L-sorbose and D-melibiose, as well as the relationship between the THz spectra and molecular vibrations, we employed density functional theory (DFT) to optimize the geometry and calculate the frequency of these molecules at room temperature using Material Studio (MS) software. Initially, geometry optimization was performed, followed by energy optimization using the Perdew-Burke-Ernzerhof (PBE) generalized gradient approximation (GGA). In order to analyze the measured data more quantitatively, we measured the sample with PXRD and also simulated the crystal structure. Figure 3 shows the PXRD spectrum samples measured by our experiments and calculated by simulation. It is found that the peak values of the samples are corresponding in theoretical calculation, which proves the rationality of the crystal structure. Figure 4A shows the crystal structure of the L-sorbose solid. Through the simulation calculation, we found that the simulated absorption peak of the L-sorbose solid is 0.65, 1.30, 1.63, and 1.98 THz, as shown in Figure 4B, which is basically consistent with the experimental peak. Note that there was no negative frequency in the calculation results. This indicates that the geometric optimization of this molecule obtained the minimum energy structure, and its vibration mode is shown in Figures 4C–4F. The calculations revealed that the absorption peaks were attributed to the vibrations of -CHOH, -CH$_2$OH, and -OH groups, as well as collective molecular vibrations or intermolecular interactions. Notably, the interaction between molecules, particularly hydrogen bonding, can influence the absorption peaks in THz radiation. As a result, the simulated absorption peaks may slightly differ from the experimentally observed peaks, such as the case of 0.65 THz. At the same time, the peaks at 1.25 THz and 1.35 THz are combined into one peak at 1.30 THz in the calculation.

Figure 5A shows the crystal structure of the D-melibiose in its solid form. Through simulation calculation, we determined that the simulated absorption peaks of D-melibiose solid were 0.85, 1.20, 1.60, 1.81 THz, as depicted in Figure 5B. These four peaks closely correspond to the experimental results, where 0.85 THz corresponds to 0.89 THz, 1.20 THz corresponds to 1.27 THz, and 1.60 and 1.81 THz directly match the experimental peaks. Therefore, these four peaks were preliminarily determined as the characteristic peaks of D-melibiose solid, and their vibration modes are shown in Figures 5C–5F, respectively.

The disparity between the experimental and simulation results can be elucidated through several factors. Firstly, because we adopt idealized crystal structures in our calculations, it is difficult to achieve in actual experimental measurements. Secondly, the absorption peaks in THz radiation can be influenced by intermolecular interactions, particularly hydrogen bonding. These interactions may not be fully captured in the

Table 1. THz vibration modes of L-Sorbose and D-Melibiose

Sample	Experimental result f/THz	Theoretical simulation f/THz	Vibration mode attribution
L-sorbose	0.61	0.65	molecular collective vibration intermolecular interaction
	1.25	1.30	-CHOH, -CH$_2$OH, -OH in-plane bending vibration
	1.63	1.63	-OH in-plane bending vibration, =O out-of-plane bending vibration, molecular collective vibration
	1.98	1.98	-OH out-of-plane bending vibration
	0.85	0.89	intermolecular interaction
D-melibiose	1.20	1.27	-CHOH, -CH$_2$OH, in-plane bending vibration
	1.60	1.66	-OH, -CHOH out-of-plane bending vibration
	1.81	1.81	-OH, -CHOH, =O in-plane bending vibration

simulation, leading to slight variations in the absorption peaks. The vibrational assignments of the two saccharides in the THz frequency range are detailed in Table 1.

THz spectra of saccharide solutions

Most saccharides in solution play a role in the life activities of living organisms; thus, we utilized a THz-TDS system combined with a micro-fluidic chip to measure the solution samples of both saccharides. In fact, water exhibits strong absorption in the THz range. Hence, we employed Equation 2 to determine the absorption coefficients of the sample (including solvent and solute) and the absorption coefficient of the solvent (deionized water). Then, take the ratio of these two absorption coefficients to obtain the relative absorption coefficient spectrum, as shown in Figures 6. Figures 6B and 6E are the absorption spectra without the data processing. It can be observed that the absorption peak of the sample is relatively small, indicating a significant influence of the solvent. However, after data processing, the relative absorption peaks become more prominent, as shown in Figures 5C and 5F, and the influence of most solvents is eliminated. Therefore, we believe that this data processing method can largely extract absorption peaks in liquid samples. Note that the THz absorption spectra of both saccharide solutions after data processing are roughly similar to the solid spectra, and the absorption peaks presented by the solid are largely present in the solution. However, the solution absorption spectra reduce the amplitude of the absorption peaks of the samples
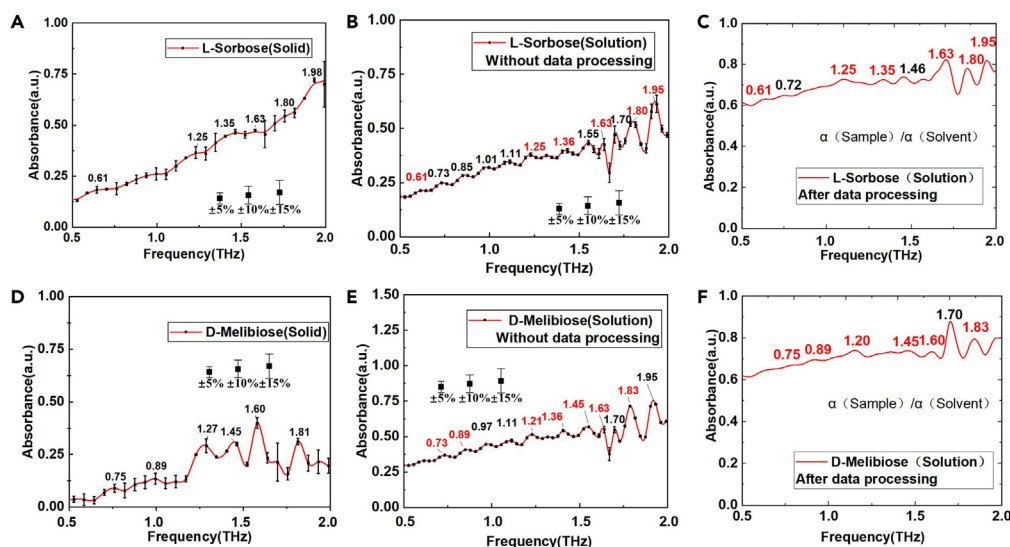

Figure 6. Absorption coefficient of L-sorbose and D-melibiose in solid and solution state
(A) Absorption coefficient spectrum of solid L-sorbose.
(B) Absorption spectrum of L-sorbose solution without data process.
(C) Absorption spectrum of L-sorbose solution after data process.
(D) Absorption coefficient spectrum of solid D-melibiose.
(E) Absorption spectrum of D-melibiose solution without data process.
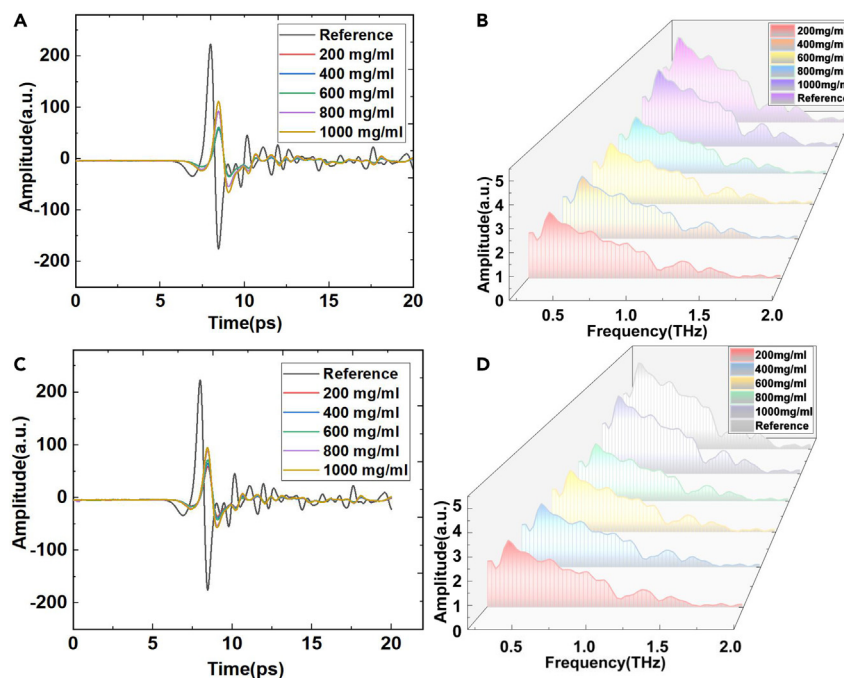(F) Absorption spectrum of D-melibiose solution after data process.

Figure 7. THz spectra of L-sorbose and D-melibiose at different concentrations
(A) Time-domain spectra of L-sorbose solutions with different concentrations.
(B) Frequency domain spectra of L-sorbose solutions with different concentrations.
(C) Time-domain spectra of different concentrations of D-melibiose solutions.
(D) Frequency domain spectra of different concentrations of D-melibiose solutions.

due to the interaction of the samples with water and the effect of high absorption by hydrogen bonding, and new absorption bands appear that are not present in the solid. Additionally, it is worth noting that the absorption band in the solution can be composed of several adjacent characteristic absorption peaks observed in the solid state. This suggests that the behavior of L-sorbose and D-melibiose molecules is significantly influenced by the presence of water molecules in the solution. Moreover, variations in intramolecular and intermolecular interactions also contribute to the differences observed in the absorption spectra between solutions and solids. In order to ensure the authenticity of the experimental data, we repeated the experiment for more than three times in each group of the aforementioned experiments.

In addition, we investigated the correlation between concentration and spectra. First, sample solutions with different concentration gradients were prepared and injected into microfluidic chips. The THz spectra of the L-sorbose and D-melibiose solutions with different concentrations were measured at room temperature. The THz time-domain spectra and frequency domain spectra are shown in Figure 7. Here we found that, with the increasing concentration of L-sorbose and D-melibiose, the time-domain spectra and frequency domain spectra were relatively enhanced, which indicates that the absorption was less and the transmittance was larger. It is clear that the THz absorption spectra of two saccharide solutions were affected by the amount of L-sorbose or D-melibiose molecules involved. Note that water molecules were present in the liquid sample; thus, the high absorption of THz will greatly affect the absorption peak of the sample. Therefore, this experiment did not compare the absorption coefficients of different concentrations.

We then selected two saccharide samples with a concentration of 1 g/mL and injected them into a microfluidic chip with a temperature control device. The control system monitored heating and temperature on the chip. The THz-TDS system acquired the measured values at 10°C intervals and generated the THz frequency domain spectra, as depicted in Figures 8A and 8C. As can be seen, the THz transmission intensity of both the L-sorbose and D-melibiose decreased gradually as the temperature increased. Note that we discharged the air into the liquid cell when injecting the samples. The data in this paper are valid because there were no air bubbles in the liquid pool to ensure that there was no liquid leakage. However, in the temperature experiment, we found that bubbles appeared in the chip when the liquid pool was continuously heated above 70°C, which indicates that evaporation affected the concentration of the sample, thereby resulting in different experimental conditions. As a result, temperature stability and temperature extreme experiments could not be performed. We selected the spectral values at 0.6 THz, as shown in Figures 8B and 8D, which both exhibit a decreasing trend with increasing temperature. Here, we obtained R^2 values of 0.99639 and 0.92877, respectively, by linear fitting calculations. The THz frequency domain spectra of the L-sorbose and D-melibiose at different temperatures showed that the THz transmission intensities decreased with increasing temperature. This is primarily due to the noncovalent bonding forces, e.g., hydrogen bonding and electrostatic force in the L-sorbose and D-melibiose, which keep the properties of the molecules stable. Solutions of L-sorbose and D-honey disaccharide are polar liquids, and the absorption
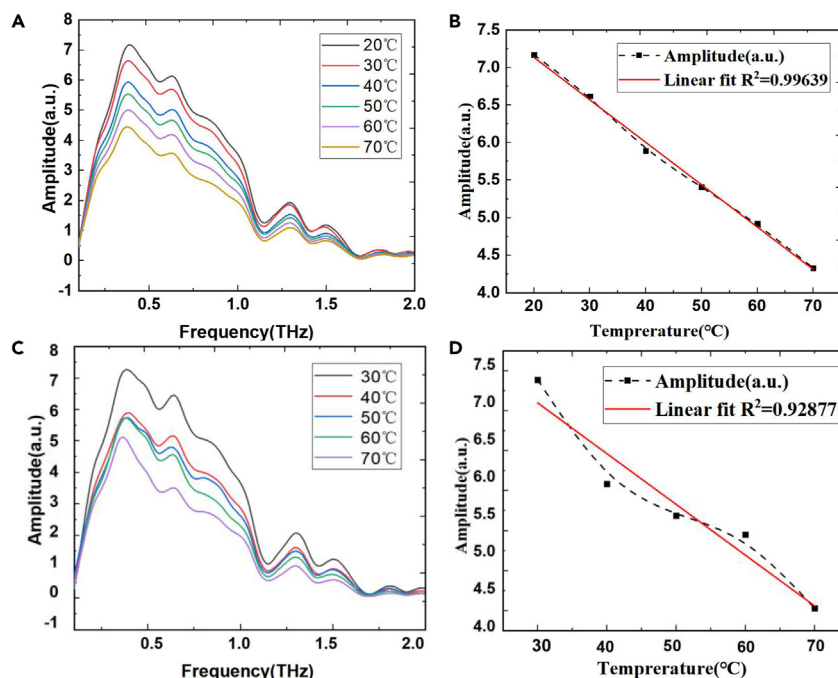
Figure 8. THz spectra of L-sorbose and D-melibiose at different temperatures

(A) Frequency domain spectra of L-sorbose at different temperatures.

(B) Linear regression diagram of peak values of L-sorbose at 0.6 THz.

(C) Frequency domain spectra of D-melibiose at different temperatures.

(D) Linear regression diagram of peak values of D-melibiose at 0.6 THz.

coefficient of polar liquids in the THz range is 10–100 times greater than that of nonpolar liquids due to hydrogen bonding interactions between the dipole and polar molecules.[20] Thus, the increased THz absorption of the L-sorbose and D-melibiose solutions was primarily caused by the dipole-molecule interactions. The relationship between the THz absorption coefficient spectrum and temperature is shown in Figure S2.

Conclusion

In this study, the vibrational absorption of L-sorbose and D-melibiose was detected and analyzed using a THz-TDS system and DFT. By measuring the vibrational absorption of the two saccharides experimentally, we found that they have different THz absorption peaks, which are in basic agreement with the anomalous dispersion of the refractive index pattern. To verify the accuracy of the experimental results, the optimized stable structures and vibrational attributions were obtained by simulation calculations, and the experimental results were in good agreement with some of the simulation results. In addition, the spectral properties of the two saccharides in solution were measured using microfluidic chip technology, and the two solid-liquid states were compared. Here, we found that the absorption bands were changed, which indicates that the intramolecular and intermolecular interactions of the L-sorbose and D-melibiose molecules were weakened due to the effect of distilled water molecules; however, the difference between their absorption spectra in the THz range remained. We then compared the spectra at different concentrations and different temperatures, and we identified a correlation between the THz absorption spectra of the same substance in solution and its concentration and temperature. These results reveal the important influence of the surrounding environment on the molecular structure and its vibrational modes. This study provides the spectral characteristics of monosaccharides and disaccharides in the low-frequency band of THz using L-sorbose and D-melibiose samples. We believe that the findings of this will lay a foundation for the application of THz in glycobiology research.

Limitations of the study

In this study, the experimental results are roughly consistent with the simulation results, but there are also small differences and offsets. The specific reasons for these differences and offsets need further experimental research.

STAR★METHODS

Detailed methods are provided in the online version of this paper and include the following:

SUPPLEMENTAL INFORMATION

Supplemental information can be found online at https://doi.org/10.1016/j.isci.2023.108602.

AUTHOR CONTRIBUTIONS

B.Z.: Investigation, Formal analysis, Validation, Writing – original draft, Writing – review & editing. Y.Z.: Conceptualization, Investigation, Methodology, Software, Formal analysis, Writing – original draft, Writing – review & editing. J.S.: Writing – review & editing, Software. B.Y.: Investigation, Software. B.P.: Investigation, Software. S.Q.: Investigation, Software. B.S.: Investigation, Resources, Project administration, Funding acquisition. C.Z.: Supervision, Project administration.

DECLARATION OF INTERESTS

The authors declare no competing interests.

REFERENCES

1. Shao, Y., Gu, W., Qiu, Y.A., Wang, S., Peng, Y., Zhu, Y., and Zhuang, S. (2020). Lipids monitoring in Scenedesmus obliquus based on terahertz technology. Biotechnol. Biofuels *13*, 161.

2. Cherkasova, O.P., Serdyukov, D.S., Ratushnyak, A.S., Nemova, E.F., Kozlov, E.N., Shidlovskii, Y.V., Zaytsev, K.I., and Tuchin, V.V. (2020). Effects of Terahertz Radiation on Living Cells: a Review. Opt. Spectrosc. *128*, 855–866.

3. Wang, Q., Xie, L., and Ying, Y. (2021). Overview of imaging methods based on terahertz time-domain spectroscopy. Appl. Spectrosc. Rev. *57*, 249–264.

4. Sarieddeen, H., Alouini, M.S., and Al-Naffouri, T.Y. (2021). An Overview of Signal Processing Techniques for Terahertz Communications. IEEE *109*, 1628–1665.

5. Zhang, L., Zhang, M., and Mujumdar, A.S. J. (2023). Terahertz Spectroscopy: A Powerful Technique for Food Drying Research. Food Rev. Int. *39*, 1733–1750.

6. Rudd, P.M., Wormald, M.R., and Dwek, R.A. (1999). Glycosylation and the Immune System. Trends Glycosci. Glycotechnol. *11*, 1–21.

7. Walther, M., Plochocka, P., Fischer, B., Helm, H., and Uhd Jepsen, P. (2002). Collective vibrational modes in biological molecules investigated by terahertz time-domain spectroscopy. Biopolymers *67*, 310–313.

8. Li, Z., Hao, Y., and Peng, R.J. (2014). Advances in the biological effects of terahertz wave radiation. Military Med. Res. *3*, 4.

9. Zebiri, I., Balieu, S., Guilleret, A., Reynaud, R., and Haudrechy, A. (2011). The Chemistry of L-Sorbose. European J. Org. Chem. *2011*, 2905–2910.

10. Giridhar, R., and Srivastava, A. (2000). Productivity enhancement in L-sorbose fermentation using oxygen vector. Enzyme Microb. Technol. *27*, 537–541.

11. Šefčovičová, J., Vikartovská, A., Pätoprstý, V., Magdolen, P., Katrlík, J., Tkac, J., and Gemeiner, P. (2009). Off-line FIA monitoring of d-sorbitol consumption during l-sorbose production using a sorbitol biosensor. Anal. Chim. Acta *644*, 68–71.

12. Giridhar, R.N., and Srivastava, A.K. (2002). Productivity improvement in l-sorbose biosynthesis by fedbatch cultivation of Gluconobacter oxydans. J. Biosci. Bioeng. *94*, 34–38.

13. Hirotsu, K., and Higuchi, T. (1976). The Conformations of Oligosaccharides. III. In The Crystal and Molecular Structure of Melibiose Monohydrate Chemischer Informationsdienst, 7The Crystal and Molecular Structure of Melibiose Monohydrate Chemischer Informationsdienst, pp. 1240–1245.

14. Fu, R., Li, Z., and Jin, B. (2010). Study on vibrational spectra of L-, D-and DL-alanine in terahertz band. Spectrosc. Spectr. Anal. *4*.

15. Zheng, Z.P., Fan, W.H., Liang, Y.Q., and Yan, H. (2012). Application of terahertz spectroscopy and molecular modeling in isomers investigation: Glucose and fructose. Opt Commun. *285*, 1868–1871.

16. Upadhya, P.C., Shen, Y.C., Davies, A.G., and Linfield, E.H. (2003). Terahertz time-domain

spectroscopy of glucose and uric Acid. J. Biol. Phys. *29*, 117–121.

17. Zhang, T., Yan, S., Hao, J., and Li, D. (2021). Experimental and Theoretical Investigations of Terahertz Spectra of the Structural Isomers: Mannose and Galactose. J. Spectrosc. *2021*, 1–9.

18. Song, C., Fan, W.H., Ding, L., Chen, X., Chen, Z.Y., and Wang, K. (2018). Terahertz and infrared characteristic absorption spectra of aqueous glucose and fructose solutions. Sci. Rep. *8*, 8964.

19. Meng, Q., Ding, J., Peng, B., Zhang, B., Qian, S., Su, B., and Zhang, C. (2022). Terahertz modulation characteristics of three nanosols under external field control based on microfluidic chip. iScience *25*, 104898.

20. Son, J. (2014). Terahertz Biomedical Science and Technology (CRC Press). Chap. 7.

21. Paul, A., George, W.H., Farhan, R., Benjamin, G., Hawkins, A., Ezekiel, S., Brian, J., and Kirby, J. (2008). Microfluidic devices for

terahertz spectroscopy of biomolecules. Opt Express *16*, 1577–1582.

22. Dorney, T.D., Baraniuk, R.G., and Mittleman, D.M. (2001). Material parameter estimation with terahertz time-domain spectroscopy. J. Opt. Soc. Am. Opt Image Sci. Vis. *18*, 1562–1571.

23. Duvillaret, L., Garet, F., and Coutaz, J.L. (1999). Highly Precise Determination of Optical Constants and Sample Thickness in Terahertz Time-Domain Spectroscopy. Appl. Optics *38*, 409–415.

STAR★METHODS

KEY RESOURCES TABLE

REAGENT or RESOURCE	SOURCE	IDENTIFIER
Chemicals, peptides, and recombinant proteins		
L-sorbose	Beijing Chemsynlab Co., Ltd.	CAS# 87-79-6
D-melibiose	Beijing Chemsynlab Co., Ltd.	CAS# 585-99-9
Deposited data		
Data	This paper	https://doi.org/10.5281/zenodo.8176767
Software and algorithms		
Origin 8	Origin Lab	https://www.originlab.com/
Materials Studio	Castep	http://www.castep.org/

RESOURCE AVAILABILITY

Lead contact

Further information and requests for resources and reagents should be directed to and will be fulfilled by the Lead Contact, Bo Su (subo75@cnu.edu.cn).

Materials availability

This study did not generate new unique reagents.

Data and code availability

- Data
  All data have been deposited at Zenodo and are publicly available as of the date of publication. DOIs are listed in the key resources table.

- Code
  This paper does not report original code.

- Any additional information required to reanalyze the data reported in this work paper is available from the lead contact upon request (subo75@cnu.edu.cn).

EXPERIMENTAL MODEL AND STUDY PARTICIPANT DETAILS

Our study does not use experimental models typical in the life sciences.

METHOD DETAILS

Experimental setup

The THz-TDS system used in the experiment is a transmission system, which consists of MaiTai femtosecond laser, chopper, THz wave generation and detection device, as shown in Figure S3. The MaiTai femtosecond laser employed in this study is a titanium sapphire laser with continuously tunable wavelengths in the range of 700–1200 nm. Its central wavelength is 800 nm, repetition frequency is 82 MHz, and the output laser power is 3.4 W. The C-995 chopper modulates femtosecond laser to generate pulse laser matched with lock-in amplifier reception. The pump beam converges to InAs crystal through the lens and the electric translation stage, and InAs crystal radiates through the semiconductor surface to generate THz pulses. After being collimated by the parabolic mirror and converged on the sample, the THz wave carrying the sample information is collected by the parabolic mirror again and collimated into the ZnTe crystal. Simultaneously, another femtosecond probe beam also reaches the ZnTe crystal, and the polarization state of the probe beam changes with the electro-optical effect modulation, so that the polarization beam splitting ratio changes after it passes through the Wollaston prism, which is detected by the differential detector. The weak current is input to the lock-in amplifier, and after amplification, shaping and phase shifting, it enters the phase-sensitive detector and the reference signal for correlation detection, which suppresses incoherent noise, thus the signal is amplified and the signal-to-noise ratio is improved. During the experiment, the relative optical path difference between pump beam and probe beam is adjusted by computer-controlled electric pan/tilt, and the time domain waveform of THz pulse is obtained by point-by-point scanning.

The experimental system achieves a signal-to-noise ratio greater than 800, with an effective spectral range of 0.2–2.0 THz, as shown in Figure S4. The scanning step size is 10 μm, the length is 3 cm, the frequency domain resolution is 37 GHz, and the time domain resolution is 66 fs.

Sample preparation

In this study, L-sorbose (99.99%, Beijing Chemsynlab Co., Ltd.) and D-melibiose (99%, Beijing Chemsynlab Co., Ltd) were used without further purification, and distilled water with a resistivity of 18.2 Ω cm was used in the experiments. The L-sorbose and D-melibiose solutions were prepared at five concentrations ranging from 0 to 1 g/mL. Polyethylene, which is a white powder with almost total transmission of THz waves and a good test preparation agent (Figure S5), was obtained from Sigma Aldrich Trading Co., Ltd. The samples were prepared by thoroughly grinding 100 mg of L-sorbose and D-melibiose under a pressure of 5 tons and mixing them with polyethylene at a ratio of 1:5 to form samples with a diameter of 1 cm and a thickness of 0.95 and 1.49 mm, respectively.

Microfluidic chip and temperature control device

To address the potential impact of liquid samples on THz absorption and ensure accurate results, a specially designed microfluidic chip was utilized in this study. Zeonor 1420R has an average transmission rate of 95% in the THz range (Figure S6) and is transparent to visible light. Additionally, it does not have absorption peaks, making it an ideal material for microfluidic chips.[21] Two Zeonor 1420R pieces were used, one as the substrate and the other as the cover sheet, separated by a 50 μm thick double-sided adhesive as an intermediate layer. A channel measuring 2 cm in length and 1 cm in width was established by removing a section of the double-sided adhesive. The substrate cover sheet was then glued, and two 1 mm radius circular holes were carved out of the cover sheet as the inlet and outlet ports. The implementation of this microfluidic chip minimizes sample loss and absorption, resulting in a cost-effective and environmentally friendly solution.

The temperature control system, depicted in Figure S7, consists of a microfluidic chip and a temperature sensor attached on the same side of the metal layer as the thermally conductive silicone. The annular heating plate is composed of alumina ceramic and has an outer diameter of 40 mm and an inner diameter of 20 mm, which is fixed on the other side of the metal plate without impeding the transmission of THz waves through the liquid pool. The temperature sensor and ceramic heater are connected by wires to a temperature controller (ST700 intelligent proportional-integral temperature controller with a rated voltage of 220 V, adjustable temperature range of 0°C–200°C, and accuracy of 0.1°C). During the experiment, the temperature controller adjusts the target temperature, and automatically regulates the rise and fall of the temperature, ultimately maintaining a constant value near the target temperature. To indirectly and qualitatively measure the temperature change characteristics of the sample, the temperature sensor measures and gives feedback on the temperature of the microfluidic chip, which reflects the temperature gradient rise.

Calculation method

To eliminate the influence of Fabry–Perot oscillation on the experiment, we used the flat-plate medium model based on the Fresnel formula proposed by Dorney to process the experimental data. In this study, the physical model of the THz optical parameters of the extracted substance proposed by Dorney was utilized to calculate the refractive index n and the absorption coefficient of the sample.[22,23] This model performs Fourier transform on the THz time-domain waveforms of the reference and transmitted samples to obtain the amplitude and phase information of the reference and transmitted sample, and it calculates the refractive index of the sample with the known sample thickness d.

$$n(\omega) = \frac{c}{\omega d}\varphi(\omega) + 1 \qquad \text{(Equation 1)}$$

Here, ω is the circular frequency, c is the speed of light in vacuum, and $\varphi(\omega)$ is the phase difference, which is calculated further to obtain the absorption coefficient.

$$\alpha(\omega) = \frac{2}{d}\ln\left\{\frac{4n(\omega)}{\rho(\omega)[n(\omega)+1]^2}\right\} \qquad \text{(Equation 2)}$$

Here, $\rho(\omega)$ is the amplitude ratio of the sample and the reference.

To analyze the experimental spectra in detail and explore the specific reasons for the formation of absorption peaks, quantum chemical simulation calculations were performed via the solid-state DFT. The specific parameters are as follows: Task: Geometry optimization and Energy; Quality: Fine; Energy cutoff: Fine, 571.4 eV; SCF Tolerance: Fine; Energy tolerances per: atom; K-point set: Fine 3 × 3×4; Relativistic treatment: koelling-Harmon. The boundary conditions are as follows: lengthA: 20, lengthB: 20, lengthC: 20, angle alpha: 90, angle beta: 90, angle gamma: 90.

QUANTIFICATION AND STATISTICAL ANALYSIS

There is no statistical analysis in this paper.

ADDITIONAL RESOURCES

We have no relevant resources.